Simulation of a Reactor Clarifier of Water Treatment Plant

Zheng-Yan Wen[a], Trinh Thi Ngan Thanh[b], Zhi-Rong Lin[b], Rome-Ming Wu[b,c,*]

[a] Department of Chemical and Materials Engineering, Tamkang University

[b] Department of Safety, Health and Environmental Engineering, Ming Chi University of Technology

[c] Center for Environmental Sustainability and Human Health, Ming Chi University of Technology

ABSTRACT

A reactor clarifier is a crucial process that enhances the performance of the subsequent process overcome water scarcity. To get satisfaction in its performance, this study used computational fluid dynamics (CFD) as a robust and cost-efficient mathematical tool for simulating the flow field and concentration changes to investigate their influences on the effluent and sludge blanket in the various situations. We propose a set of models for comparison between the different flow models. Discrete phase model (DPM) is used to realize the particle trajectory. A defined viscosity function of the sludge blanket is also used to try to simulate more clearly the real site operation. The results show that the high concentration of sludge blanket is more stable and less susceptible to disturbance. The sludge blanket may accumulate inside the reaction hood with higher concentration. Based on the provided model, it can be successfully used as the design of the reaction hood.

Keywords: Clarifier, computational fluid dynamics, water treatment, 3D simulation, water scarcity

1. Introduction

Global water scarcity is facing enormous challenges. One of them is treating high turbidity water in the water plants. In Taiwan, this environmental issue frequently occurred during the rainy season. Due to the typhoons accompanied by heavy rain, the intake turbidity levels could increase from the daily load to very high level [1]. To deal with this sudden change of turbidity in water raw, the increase of flocculant in certain pH values is a common treatment method; however, it leads to additional chemical cost, increase sludge production and uncontrollable sludge blanket height. Besides, the conventional coagulation-clarification process requiring multiple tanks and pipework occupies a large area. This is not appropriate in Taiwan's condition.

A reactor clarifier combining two principal functions that are flocculation and clarification provides the most economical solution for treating turbidity [2]. This single basin facilitates the contact and mixing between chemicals and solids to form insoluble coagulated flocs and then sink toward the bottom of the clarifier; sludge blanket captures the impurities in the raw water. The clarified water rises to the surface outside the reaction well and is transferred to the filter unit. In addition, it could have a surface loading 2-3 times higher than the conventional treatment process.

The sludge blanket is the core of the reaction clarifier and control conditions are particularly important [3-4]. The stability of the sludge blanket is controlled by the upward velocity and the settling velocity of the flocs [5-6]. To maintain the stability of the sludge blanket, the operational control must prevent sludge washout into the clarified water [7]. Thus, many studies have been attempted to comprehensively simulate the flow velocity and solids distribution in the clarifier.

The solid flux theory and force balance have been extensively applied in the design and operation of full-scale settling tanks [8-9]. Takacs et al. studied a dynamic model of the clarification-thickening process based on one-dimensional mass balance and the solid flux concept to characterize the settling velocity of suspended solid under a variety of conditions [10]. However, the limitations of a one-dimensional ideal model are only required under the dynamic condition and unpredictable for effluent suspended solids [11]. DeClercq et al. proposed a latter one-dimensional clarifier model based on actual plant data. Although this model was not possible to predict the concentration at the surface, it could accurately describe the sludge profile and blanket height [12]. Instead of using a one-dimensional model, Wett used the solid flux theory to perform a three-layer (clarification, hindered settling, and compression zone) model to give an obvious description of sludge blanket variations [13]. Other related studies that simulate clarifiers in mathematical models [14-18].

To date, the multiphase flow studies have developed in the application of Computational Fluid Dynamics (CFD) [19,20]. 3D models that have seen steady growth in CFD are used to provide an accurate simulation of the clarifier [21-23]. Recent CFD models have provided new insight and better designs as a robust tool to many applications. [24-28] Goula et al. used CFD to assess the effect of the retrofitting a vertical baffle of a sedimentation tank to improve the solid settling [29]. Shahrokhi et al studied the effect of baffles on sedimentation tanks; from the CFD simulation result of kinetic energy and maximum velocity magnitude, uniform velocity vector inside the settling zone could indicate better sedimentation effect [30]. Tarpagkou and Pantokratoras employed CFD in order to describe the 3D hydrodynamics and flow behavior in a sedimentation tank [31]. Das et al. applied CFD to analyzing the ramifications of the clarifier geometry on performance. The CFD model was used to investigate the optimal modifications in order to improve the clarifier performance [32]. Morse extended an established 2D CFD clarifier model formulation into a 3D CFD model with additional changes including incorporation of a two-equation, turbulent production and dissipation rate model (k-ε), and a generalized velocity parameter, G, for use in the flocculation sub-model [33]. Gao and Stenstrom studied the main clarifier design factors by using a 3D model with input design parameters from several previous studies so that model outputs were compared to field data and results in the original studies [34]. In this work, three dimensional simulation of a clarifier is applied to obtain flow field and concentration changes and their influences on the effluent and sludge blanket were studied. Turbulent modeling was applied on all fluid simulated in the clarifier. Eulerian multiphase modeling was used to distinguish water and sludge blanket in the clarifier. Finally, discrete phase modeling was used to trace the particle in the clarifier. Based on the provided model, it can be used as the design of the reaction hood to improve the efficiency of the clarifier.

2. Governing equations and boundary conditions

The feature geometry of the clarifier is described in **Figure 1**. In this study, the model for the clarifier is rectangular with dimensions of 19 m, 19 m, and 5.5 m. The internal structure includes a conical hollow with the upper and lower diameters of 8 and 13 m, the inner space is the second reaction chamber. The draft tube with a diameter of 2.4 m and a height of 3.7 m is known as the reaction well. This is also the first reaction chamber; the inlet pipe with a diameter of 0.9 m and the length of 8.3 m is connected to the draft tube. The impeller has a diameter of 3.2 m with 16 blades in the top center of the clarifier. The boundary condition is no-slip wall condition.

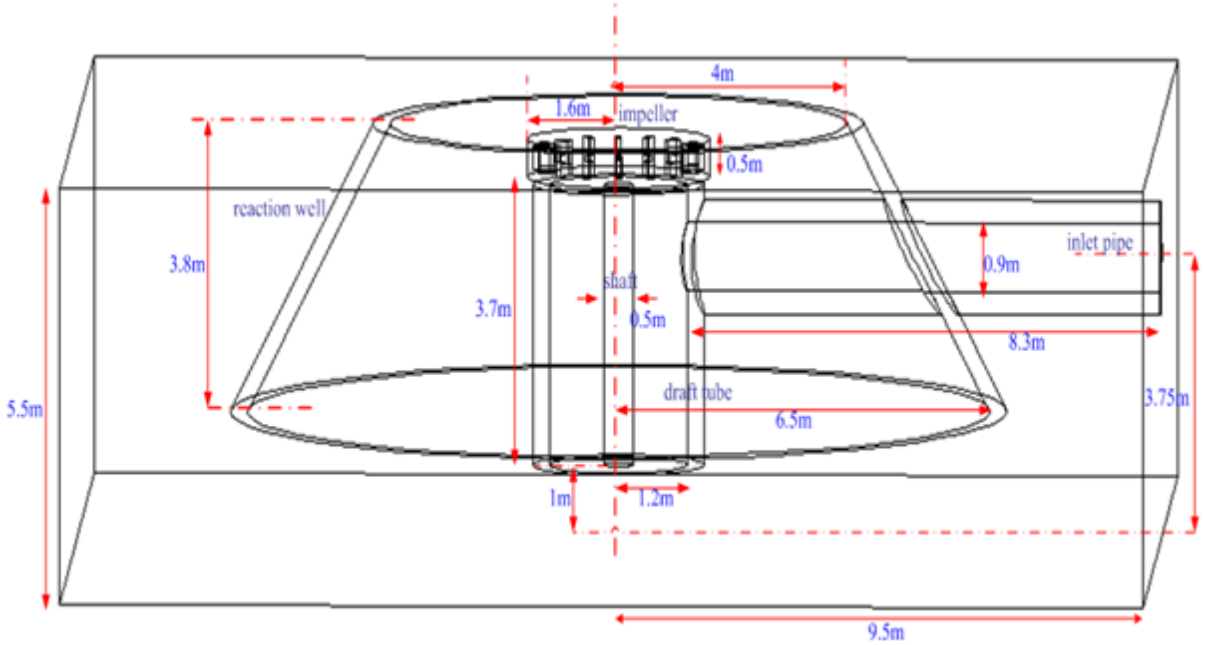

Figure 1. Geometry of the reaction clarifier

2.1 k-ε turbulent modeling

This model solves the conservation of turbulent kinetic energy *k*:

$$\frac{\partial}{\partial t}(\rho_m k) + \nabla \cdot (\rho_m \vec{u}_m k) = \nabla \cdot \left(\frac{\mu_{t,m}}{\sigma_k} \nabla k\right) + G_{k,m} - \rho_m \varepsilon \quad (1)$$

and its dissipation rate ε

$$\frac{\partial}{\partial t}(\rho_m \varepsilon) + \nabla \cdot (\rho_m \overrightarrow{u_m} \varepsilon) = \nabla \cdot \left(\frac{\mu_{t,m}}{\sigma_\varepsilon} \nabla \varepsilon\right) + \frac{\varepsilon}{k}\left(C_{1\varepsilon} G_{k,m} - C_{2\varepsilon} \rho_m \varepsilon\right) \quad (2)$$

Where G_k represents the generation of turbulence kinetic energy due to the mean velocity gradients; $C_{1\varepsilon}$, $C_{2\varepsilon}$ are the constants; σ_k , σ_ε are the turbulent Prandtl numbers for *k* and ε; ρ_m is mixture density; $\overrightarrow{u_m}$ is mixture velocity.

2.2 Eulerian Multiphase Model

2.2.1 Volume fraction

It represents the space occupied by each phase in the fluid and conforms to the law of conservation of mass and momentum. The volume of any phase is defined as:

$$V_q = \int_v \alpha_q dV \quad (3)$$

where $\sum_{q=1}^{n} \alpha_q = 1$. The effective density for any phase is:

$$\hat{\rho}_q = \alpha_q \rho_q \tag{4}$$

where ρ_q is the physical density of the phase *q*.

2.2.2 Conservation equation

With mass conservation, the continuous equation can be written as:

$$\frac{\partial}{\partial t}(\alpha_l \rho_l) + \nabla \cdot (\alpha_l \rho_l \vec{v}_l) = 0 \tag{5}$$

where $\vec{v}_l$ is the velocity of the liquid phase *l*.

Under momentum conservation, the momentum balance of the liquid phase is as follows:

$$\frac{\partial}{\partial t}(\alpha_l \rho_l \vec{v}_l) + \nabla \cdot (\alpha_l \rho_l \vec{v}_l \vec{v}_l) = -\alpha_l \nabla p + \nabla \cdot \bar{\bar{\tau}}_l + \alpha_l \rho_l \vec{g} + \sum_{L=1}^{n} (K_{Ll}(\vec{v}_L - \vec{v}_l) + \dot{m}_{Ll}\vec{v}_{Ll} - \dot{m}_{lL}\vec{v}_{lL}) \tag{6}$$

where $\bar{\bar{\tau}}_l$ The stress-strain tensor for the liquid phase l is expressed as follows:

$$\bar{\bar{\tau}}_l = \alpha_l \mu_l (\nabla \vec{v}_l + \nabla \vec{v}_l^T) + \alpha_l (\lambda_l - \frac{2}{3}\mu_l) \nabla \cdot \vec{v}_l \bar{\bar{I}} \tag{7}$$

where μ_l and λ_l are the shear and bulk viscosity of water phase. $\vec{g}$ is the acceleration due to gravity. $\vec{v}_{Ll}$ is the interphase velocity, defined as follows. If, $\vec{v}_{Ll} = \vec{v}_L$; if $\dot{m}_{Ll} < 0$, $\vec{v}_{Ll} = \vec{v}_l$. $\vec{R}_{Ll}$ is the force acting from phase to phase, and depends on friction, pressure, cohesion and other effects, and follows the conditions of $\vec{R}_{Ll} = -\vec{R}_{lL}$ and $\vec{R}_{ll} = 0$, which are expressed as follows:

$$\sum_{L=1}^{n} \vec{R}_{Ll} = \sum_{L=1}^{n} K_{Ll}(\vec{v}_L - \vec{v}_l) \tag{8}$$

where $K_{Ll}(= K_{lL})$ is the phase-to-phase momentum exchange coefficient.

The volume fraction of each phase in the fluid is expressed as follows:

$$\frac{1}{\rho_{rq}}\left(\frac{\partial}{\partial t}(\alpha_q \rho_q) + \nabla \cdot (\alpha_q \rho_q \vec{v}_q) = (\sum_{p=1}^{n} \dot{m}_{pq} - \dot{m}_{qp})\right) \tag{9}$$

where ρ_{rq} is the reference density or the volume average density in the solution range.

A multi-fluid granular model is used to describe the liquid-solid mixing behavior. The momentum equation for the solid phase is as follows:

$$\frac{\partial}{\partial t}(\alpha_s \rho_s \vec{v}_s) + \nabla \cdot (\alpha_s \rho_s \vec{v}_s \vec{v}_s) = -\alpha_s \nabla p - \nabla p_s + \nabla \cdot \bar{\bar{\tau}}_s + \alpha_s \rho_s \vec{g} + \sum_{l=1}^{N} (K_{ls}(\vec{v}_l - \vec{v}_s) + \dot{m}_{ls}\vec{v}_{ls} - \dot{m}_{sl}\vec{v}_{sl}) \tag{10}$$

Where p_s is solids pressure, K_{ls} is the momentum exchange coefficient between liquid phase l and solid phase s, ∇p_s is solid pressure that is composed of the kinetic energy term and the collision of the second phase particles.

2.3 Discrete Phase Models

2.3.1 Equations of Motion for Particle

The particle's force balance equation is as follows:

$$\frac{du_p}{dt} = F_D(u - u_p) + \frac{g_x(\rho_p - \rho)}{\rho_p} + F_x \quad (11)$$

Among them,

$\frac{g_x(\rho_p-\rho)}{\rho_p}$ is gravity effect, $F_D(u - u_p)$ is the drag of the particle, $F_D = \frac{18\mu}{\rho_p d_p^2}\frac{C_D \mathrm{Re}}{24}$,

where u is the fluid velocity, u_p the particle velocity, μ is the molecular viscosity of the fluid, ρ is the fluid density, ρ_p is the density of the particle, d_p is the particle diameter.

Re is the relative Reynolds number, which is defined as follows:

$$\mathrm{Re} \equiv \frac{\rho d_p |u_p - u|}{\mu} \quad (12)$$

C_D is the drag force coefficient.

For grain size ranging from 1 to 10 μm, the Stokes' drag force formula is used, F_D which is defined as follows:

$$F_D = \frac{18\mu}{d_p^2 \rho_p C_c} \quad (13)$$

C_c is the correction factor for the Stokes' drag force formula, defined as follows:

$$C_c = 1 + \frac{2\lambda}{d_p}\left(1.257 + 0.4e^{-\left(1.1d_p/2\lambda\right)}\right)$$

λ is the mean free path of the molecule.

2.4 User Defined Function

This study uses the material property (DEFINE_PROPERTY) to perform the material property calculation on the grid of the specified area. The custom viscosity formula is Casson equation, and its equation is as follows:

$$\mu = \left(\frac{K_1}{\dot{\gamma}^{1/2}} + K_2\right)^2 \quad (14)$$

Where $\dot{\gamma}$ is shear rate, K_1 is Casson yield stress parameter.

3. Results and Discussion

This study uses the Fluent software simulation for the following control conditions to reflect the flow field analysis, concentration change of raw water, and sludge blanket in the clarification tank. The symbols are listed in **Table 1**. It also proposes a set of models for comparison with multiphase turbulent flow models.

Table 1. Codes of various control conditions

Symbol	Initial blanket solid volume fraction (-)	Blade rotation rate (rad/s)	Initial blanket height (m)
OG	C=0.05	R=0.9 rad/s	Z=2 m
C01	C=0.1	R=0.9 rad/s	Z=2 m
C0005	C=0.005	R=0.9 rad/s	Z=2 m
R03	C=0.05	R=0.3 rad/s	Z=2 m
R01	C=0.05	R=0.1 rad/s	Z=2 m
Z3	C=0.05	R=0.9 rad/s	Z=3 m
Z1	C=0.05	R=0.9 rad/s	Z=1 m
Z3R03	C=0.05	R=0.3 rad/s	Z=3 m

3.1 Flow field analysis of reaction clarifier in the initial operating conditions.

Inlet water flowing into the draft tube is separated into two mobile phases: One is the water phase, the other one is the solid phase. The initial operating conditions of the reaction clarifier (referred to as OG) are illustrated in Figure 2. The contour of the volume fraction of solids on a cross-section of the plane y = 0 is divided into 21 color scales. At the time t = 0, the inlet water has a solid volume fraction of 0.05, a flow rate of 0.3 m/s. A rotation speed of the impeller is 0.9 rad/s according to real site operations. At the tank bottom, the sludge blanket shown in the red color is about 2 m with a solid volume fraction of 0.5. The area between water and sludge blanket represented by green-yellow is the solid-liquid interface.

Figure 2 is the changes in solid volume fraction over time for OG on the plane y = 0. As the rotation of the impeller, strong mixing may bring bottom settled particles back to the surface and disturb the stability of fluid inside the clarifier. It can be seen from the figure that there is one inward rotating vortex in the left reaction hood and one at the bottom of the right reaction hood.

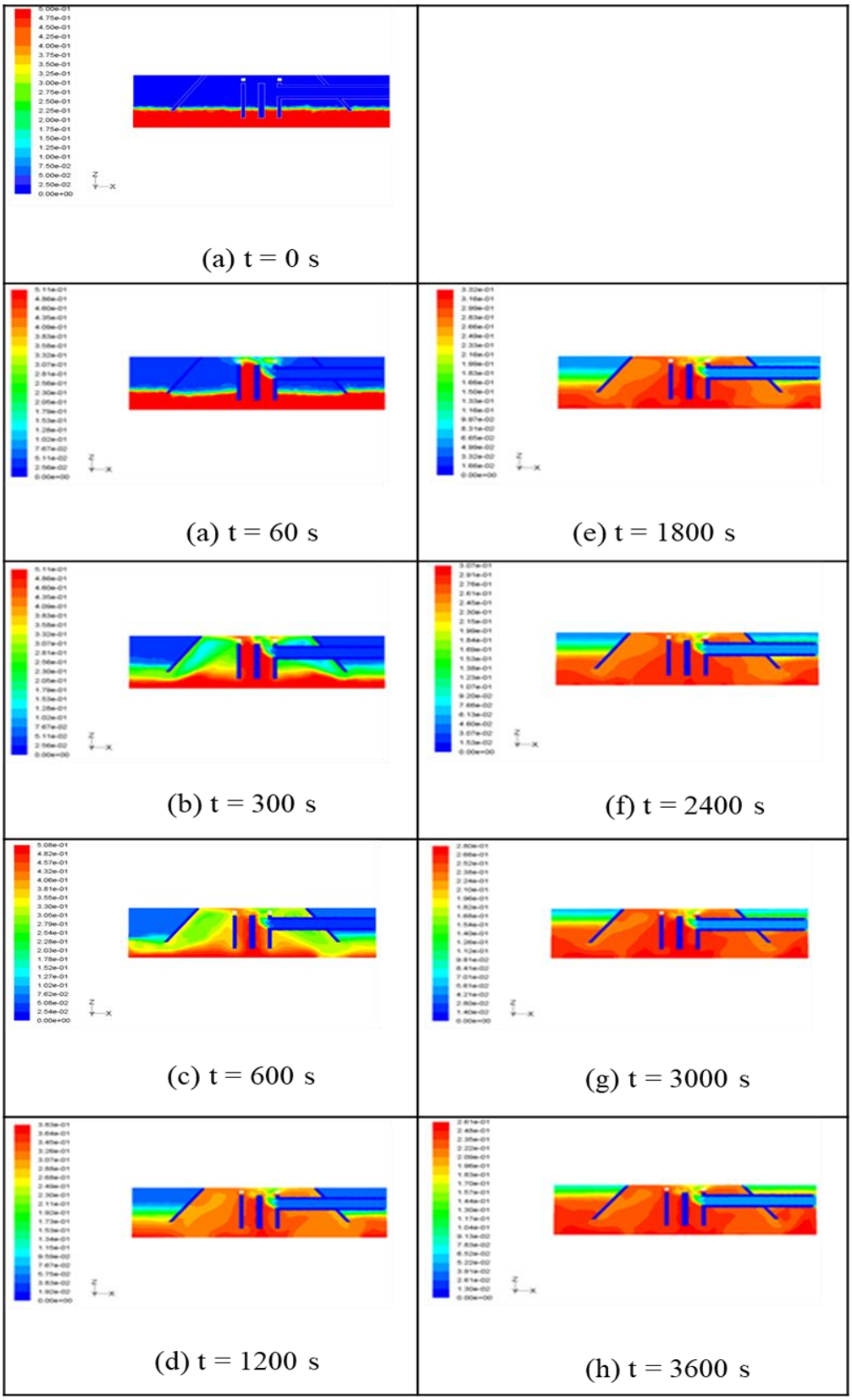

Figure 2. The change of solid volume fraction over time for OG on the plane y = 0.

3.2 Influence of different inlet water concentration on effluent quality and sludge blank

There are two different inlet water concentrations that are studied: c = 0.1 (referred to as C01) and c = 0.005 (referred to as C0005).

Figure 3 and 4 displays the contour of solid volume fraction when inlet water concentration is 0.1 and 0.005, respectively. As shown in Figure 2, the reaction hood can properly contain the flocs inside it.

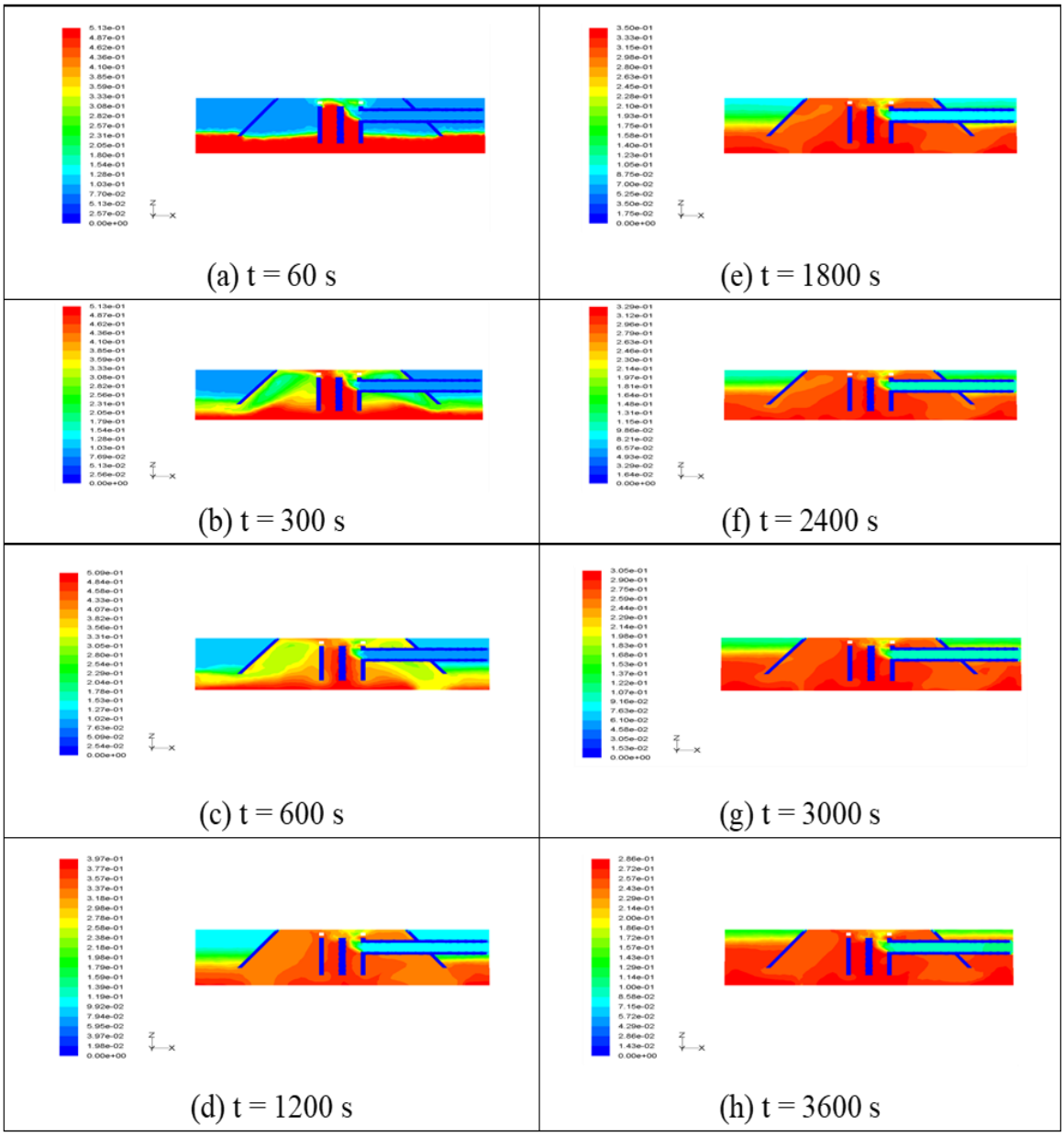

Figure 3. The change of solid volume fraction with time for C=0.1 on the plane y = 0.

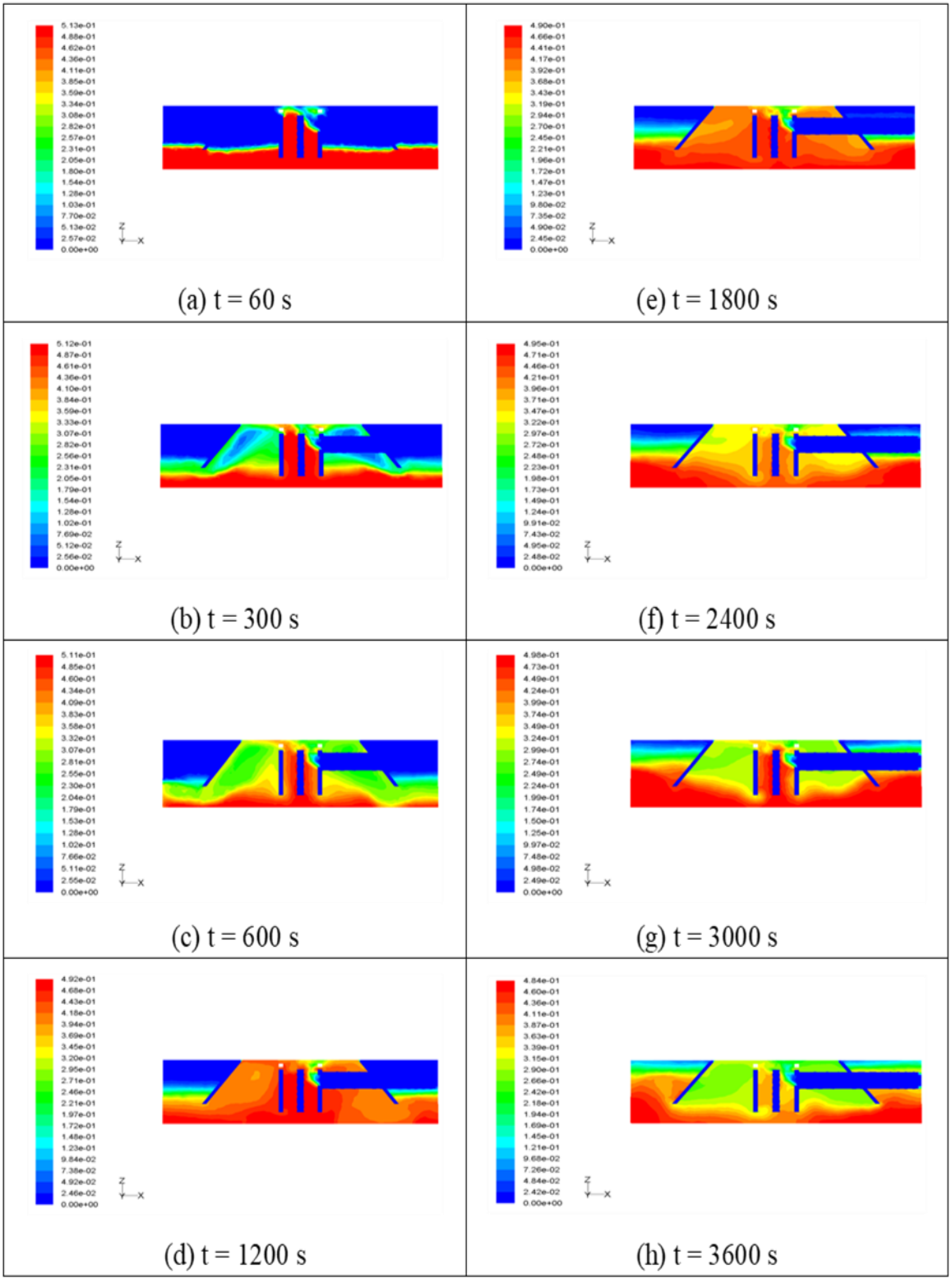

Figure 4. The change of solid volume fraction over time for C=0.005 on the plane y = 0

There are built-in modes that integrate the total volume of the solid phase. Figure 5 shows the trend of the average volume fraction of solids in the effluent. From t = 60 s to t = 1800 s (OG), the solid volume fraction of the effluent is nearly flat at about 0.05. From t = 1800 s to t = 2400 s, it begins to rise slightly because of the formation of flocs in the clarifier. After t = 2400 s, the trend graph surges dramatically from 0.052 to 0.086, showing that the water quality declined slightly within 1200 s.

From t = 60 s to t = 1800 s (C01), the quality of the effluent remains stable at about 0.101; however, it begins to rise slightly to 0.103 from t = 1800 s to 2400 s. The main cause of the increase is that the solid-liquid interface below the effluent surface has expanded significantly and the clarification tank is full of sludge particles over time. After t = 2400 s, the trend goes up considerably, the solid volume fraction increases from 0.103 to 0.135. When the inlet water concentrations is c = 0.005, the effluent increases dramatically from 0.005 to 0.11 after 2400 s.

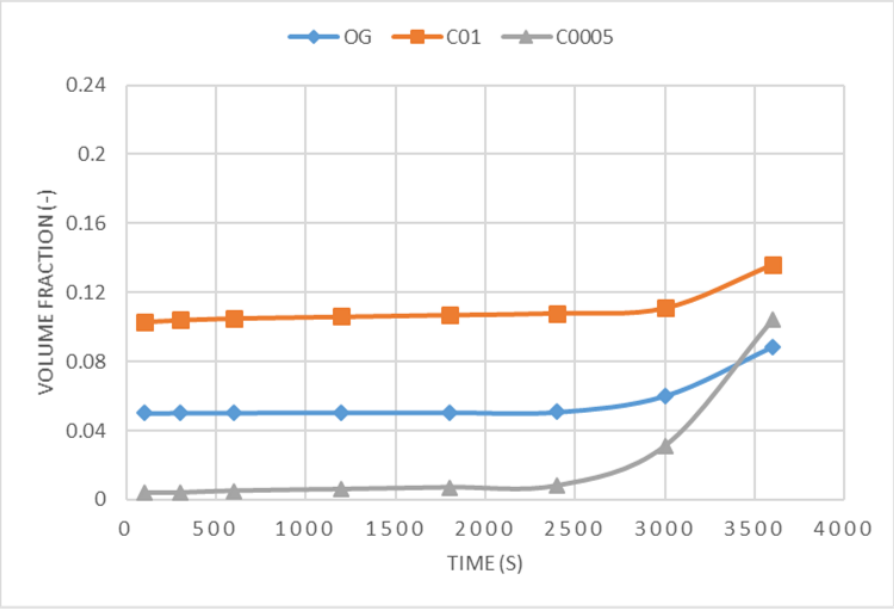

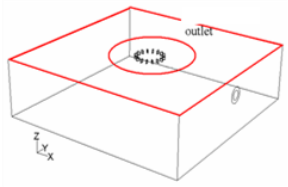

Figure 5. The trend of the average volume fraction of solids in the effluent (C= 0.1)

3.3 Impact of different impeller speeds on water quality and sludge blanket

In this case, to predict the influence of the impeller rotational speed on water quality and sludge blanket, there are two changes in the impeller speed: 0.1 rad/s (referred to as R01) and 0.3 rad/s (referred to as R03). Figure 6 and 7 show the solid volume fraction of the impeller rotating speed at 0.1 and 0.3 rad/s as a function of time. Due to the decrease of the impeller speed to 0.1 rad/s (Fig. 6), from t = 60 to t = 600 s,

there is still no obvious disturbance and the height and structure of the sludge blanket have not changed markedly. Between t = 1200 s and t = 2400 s, the second reaction chamber begins to be filled with flocs and the sludge blanket begins to loosen. From t = 3000 s to t = 3600 s, the solid-liquid interface is almost disappeared and the sludge blanket in the clarification tank stably maintains a complete structure.

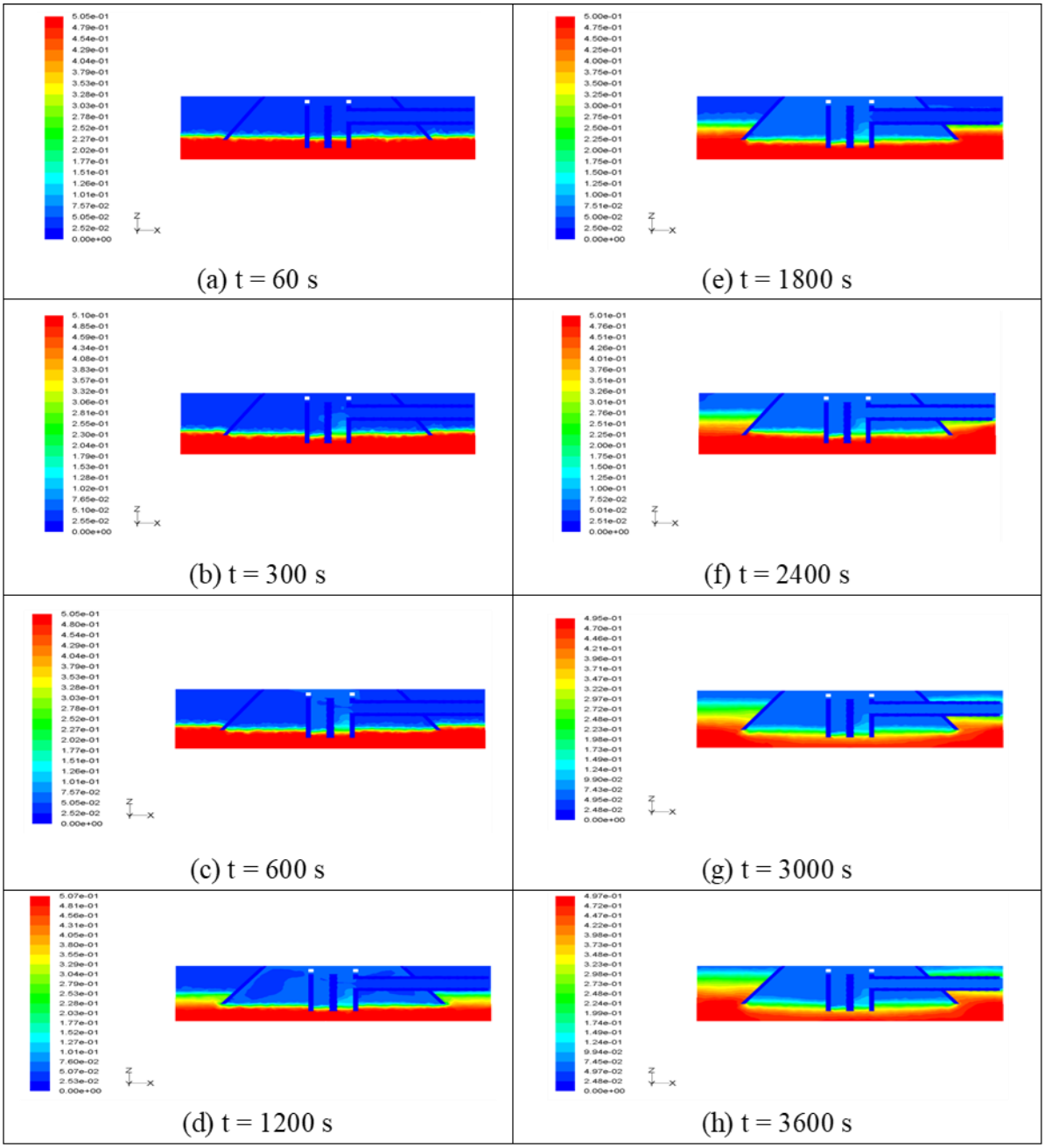

Figure 6. The change of solid volume fraction over time for R01 on the plane y = 0

Figure 7 shows the change in solid volume fraction with time of the impeller rotating speed of 0.3 rad/s. As displayed in this figure, the quality of effluent is lower than the modification of the impeller speed R01. The quality of the effluent declines by 0.01.

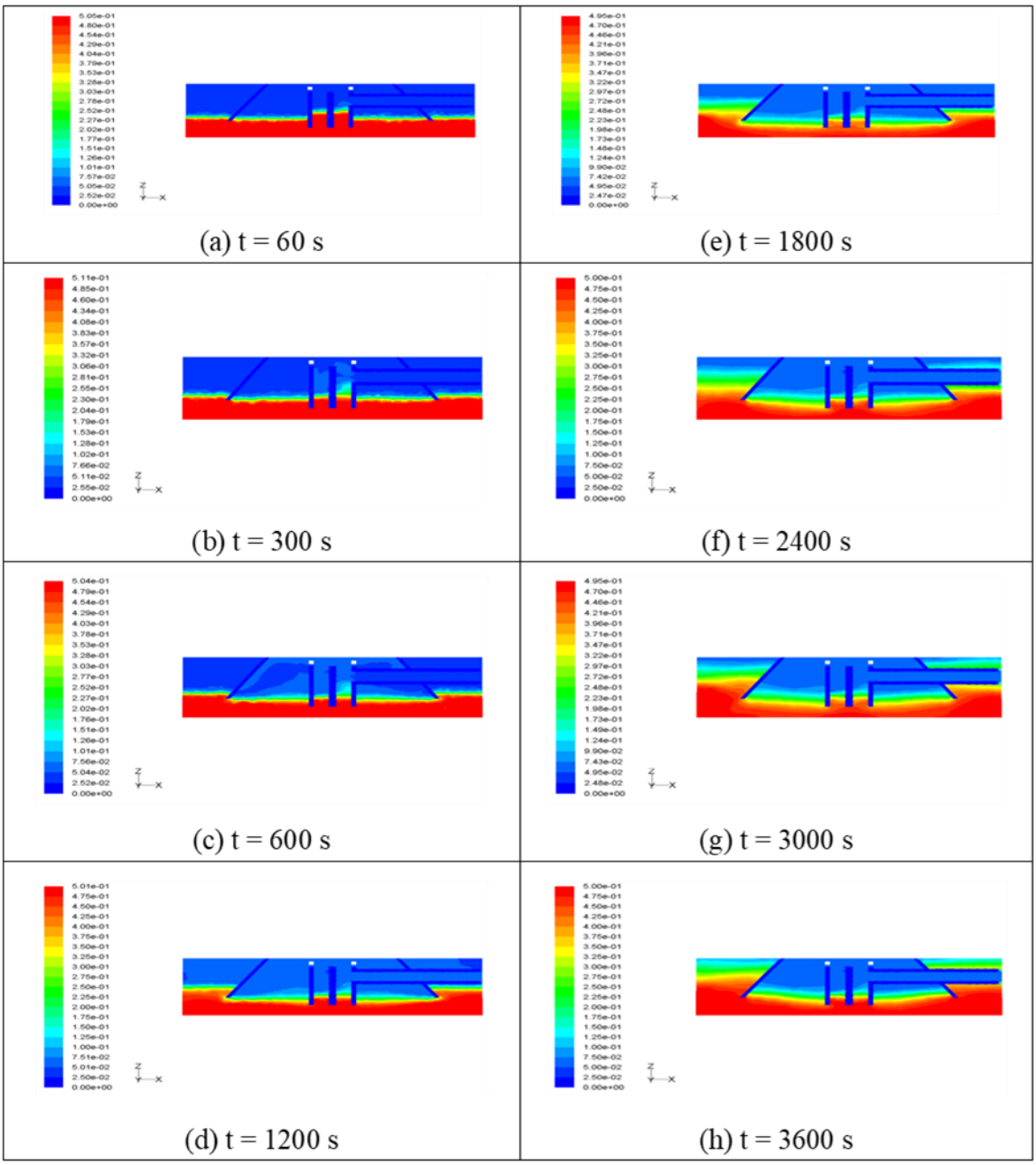

Figure 7. The change of solid volume fraction over time for R03 on the plane y = 0

Figure 8 shows the trend of the average volume fraction of solids in the effluent. From t = 60 s to t = 2400 s, the quality of effluent is stably maintained at about 0.05. After t = 2400 s, the trend rises sharply, and the solid volume fraction rises from 0.05 to 0.11, showing that the water quality has declined significantly within 1200 s.

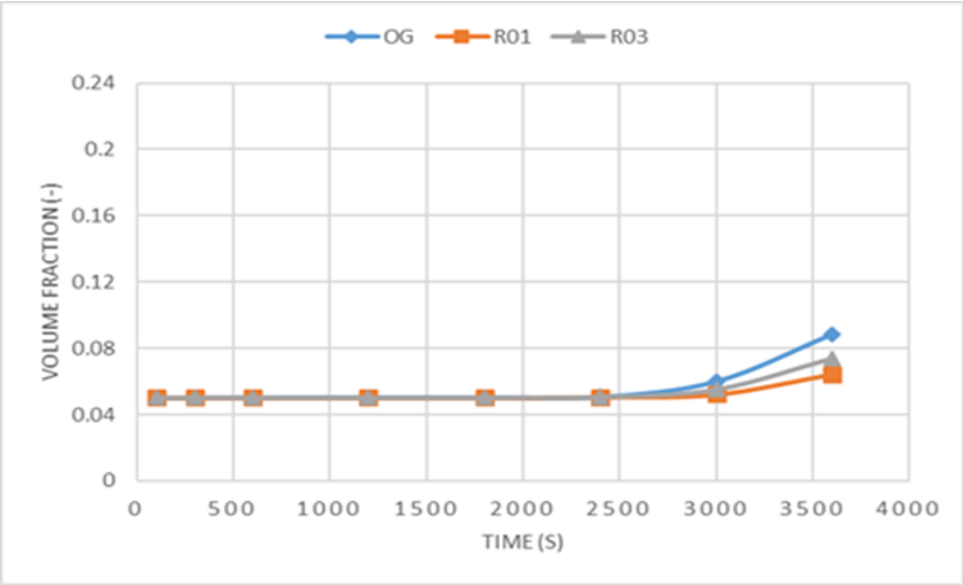

Figure 8. Trend of average volume fraction of solids in the effluent of R01

Compared with Zhang et al. [2], it is equivalent to 200 μm particles trapped in its cone-plate clarifier, resulting in about 80% SS removal.

3.4 Influence of the height of the sludge blanket on the quality of the water and the sludge blanket

To explore different sludge blanket heights and compare them with the flow field of OG (sludge blanket height of z = 2 m), hereafter shows the results of z = 1 m (referred to as Z1) and z = 3 m (referred to as Z3), with the same other operating conditions.

Figure 9 shows the trend of the average volume fraction of solids in the effluent. From t = 60 s to t = 1800 s, the quality remains stable at about 0.051. When t = 2400 s, the solid volume fraction rises to 0.08 (OG). From t = 2400 s to t = 3600 s, the solid volume fraction goes up from 0.082 to 0.22 within 1200 s (Z3). From t = 60 s to t = 2400 s, the quality of the effluent is stably maintained at about 0.051. From t = 2400 s to t = 3600 s, the solid volume fraction rises from 0.051 to 0.0601. The effluent quality decreases slightly by 0.0091 within 1200 s (Z1).

At 1800 s, solid volume fraction 0.05 is about 6.6 mg/L for 100 μm particle (ρ=1050 kg/m^3). Compare with Kolpakova et al. [3], their data is 2.5 mg/L. The reason

why our data is 2.6 times higher is that the clarifier is a hydrodynamic type. Theirs is a gravity type.

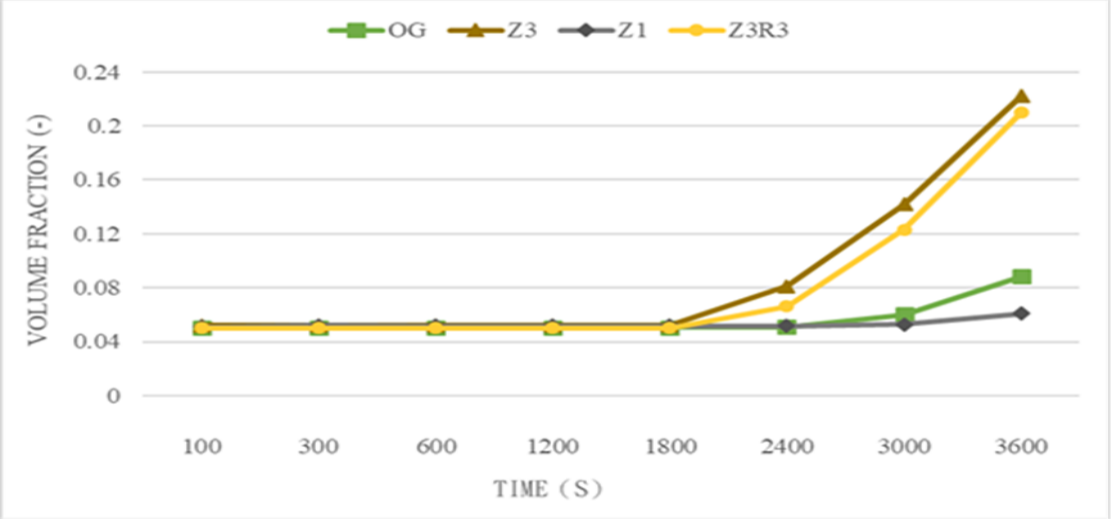

Figure 9. The trend of volume fractions with different sludge blanket heights

Figure 10 also depicts a comparison of the solid volume fractions of Z3R03 and Z3 on the z = 2 plane at t = 600 s and t = 2400 s. From Fig. 10, it can be seen that the quality of Z3 effluent after t = 1800 s decays faster than Z3R03. Because of the slowness of impeller rotating speed in Z3R03, it leads to the sludge blanket to rising less than Z3, thus the effluent quality declines slowly.

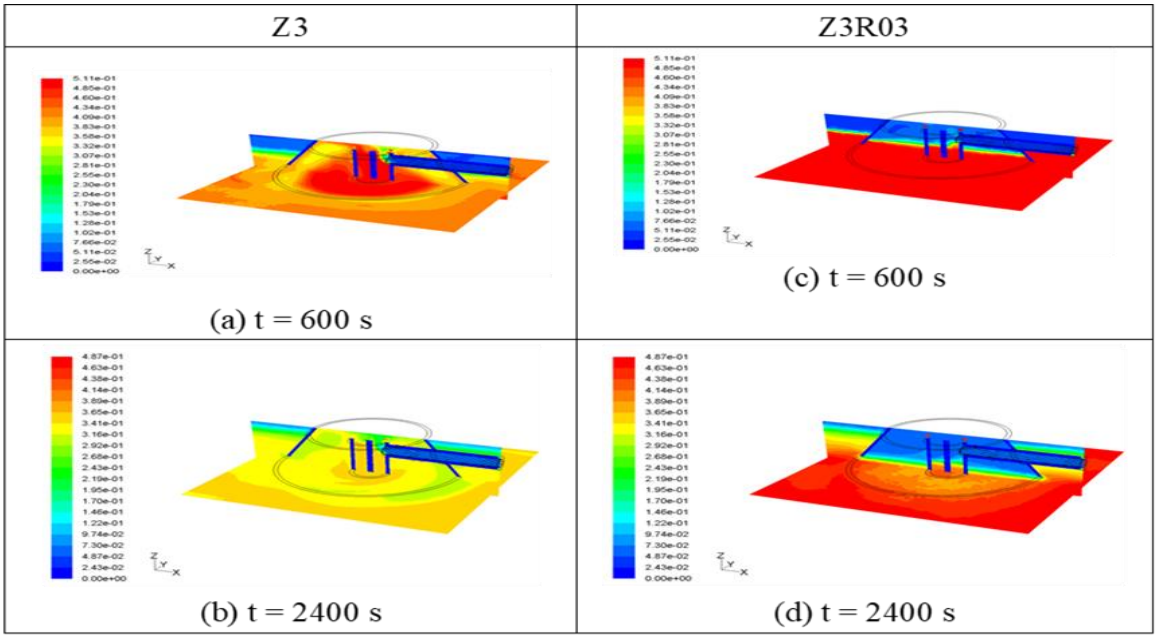

Figure 10. A comparison of Z3R03 and Z3 solid volume fractions at 600 and 2400 s

3.5 Using Discrete Phase Model to Estimate Particle Direction in Flow Field

The Discrete Phase Model (DPM) is used of injecting a few particles into an OG flow field, and observing its running trajectory to learn the conditions that the third phase particles may suffer in the process of walking in the flow field. In this study, 24 particles were injected into the OG flow field, with t = 3600 s and the injection position is the same as the position where the raw water entered the clarifier. Figure 11 shows the total time to be taken by the 21 pellets from feeding to the end of the operation. The minimum value is 2955 s, the maximum value is 19650 s, and the average of the overall time is 5557.81 s. Figure 11 is the overall time required for a single particle to orbit a flow field. One of the methods for maintaining flocs in the reaction hood is a time extension to improve the filtering effect of the reaction clarifier, because the longer the time is, the more flocs can be captured by the sludge blanket.

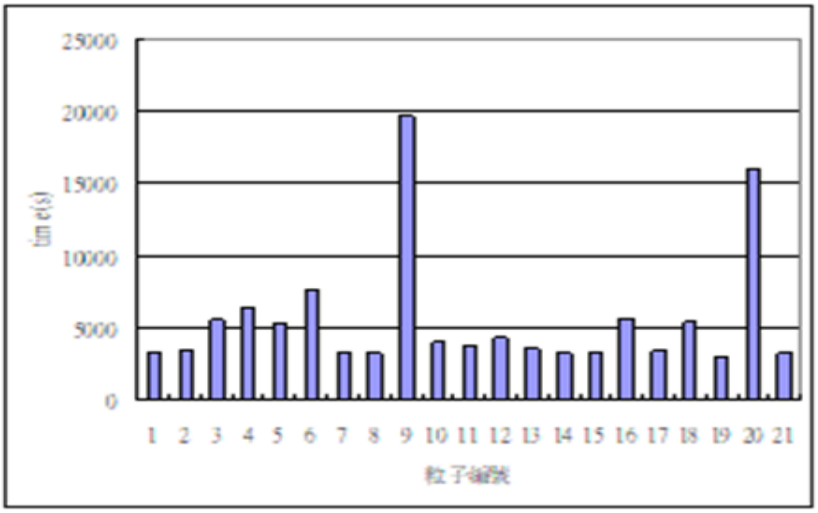

Figure 11. Overall time required for a single particle to orbit a flow field.

Figure 12 shows the time taken for the 21 particles to flow from the feed tube to the reaction hood in the flow field. The minimum value of the particles is 70 s, the maximum time is 1550 s, and the average time is 276 s. Figure 13 is the trajectory of the particles from the feeding tube into the bypass flow field and then leave the reaction hood. From these trajectory charts, it can be observed that all the particles leave the reaction hood from the right half of the reaction hood that results in the unbalance of the amount of particles in and out of the reaction hood. The time the particles spend in the reaction hood is very short, on average 251 s. Therefore, it is desired to change the geometry of the reaction hood to improve the position where the particles leave the reaction hood and extend the time that the particles are inside the reaction hood.

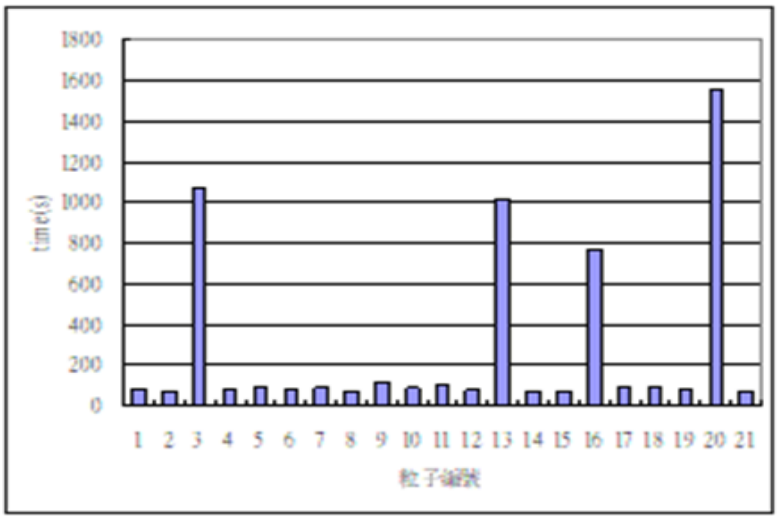

Figure 12. Time required for a single particle to leave the hood

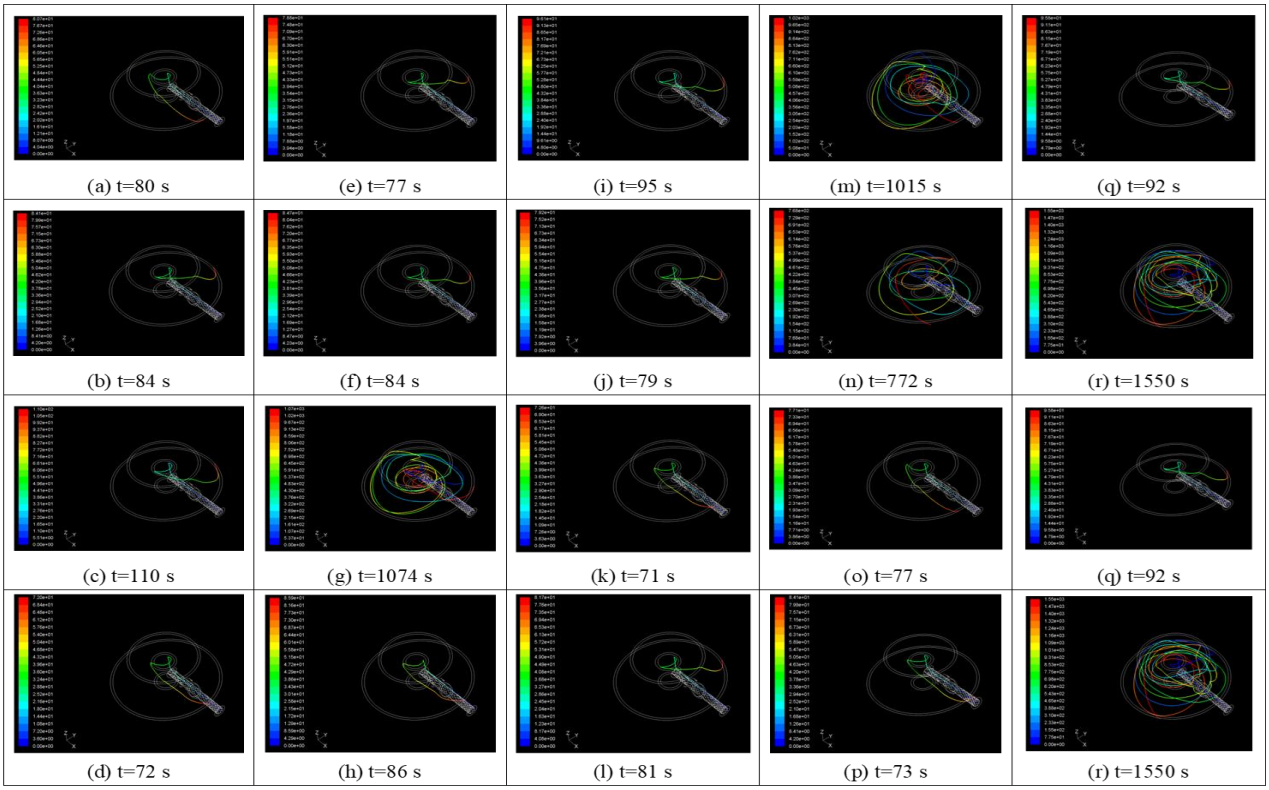

Figure 13. Single trajectory of each particle.

3.6 Effect of changing the geometry of the reaction hood on the particle flow direction

In order to prevent the particles from leaking out of the right side of the reaction hood first, a half of the right side is extended 70 cm downward in a vertical direction. There is no change in the operating condition. Figure 14 is the change of solid volume fraction of the new reaction hood (referred to as NRW) over time. Figure 15 shows a comparison of the solid volume fractions of OG and NRW on the y = 0 plane at t = 600 s and t = 2400 s. At t = 600 s, OG has a green and orange distribution with a concentration of about 0.279 to 0.4 in the reaction chamber and sludge blanket, while NRW has a light green and yellow distribution with a concentration of about 0.279 to 0.381. Both effluent qualities were maintained at 0.05 to 0.076.

At t = 2400 s, the reaction chamber and sludge blanket of OG shows orange and orange-red with a concentration of 0.245 to 0.291 with unchanged solid-liquid interface. NRW presents a light orange and orange distribution with a concentration of about 0.245 to 0.276 without the solid-liquid interface.

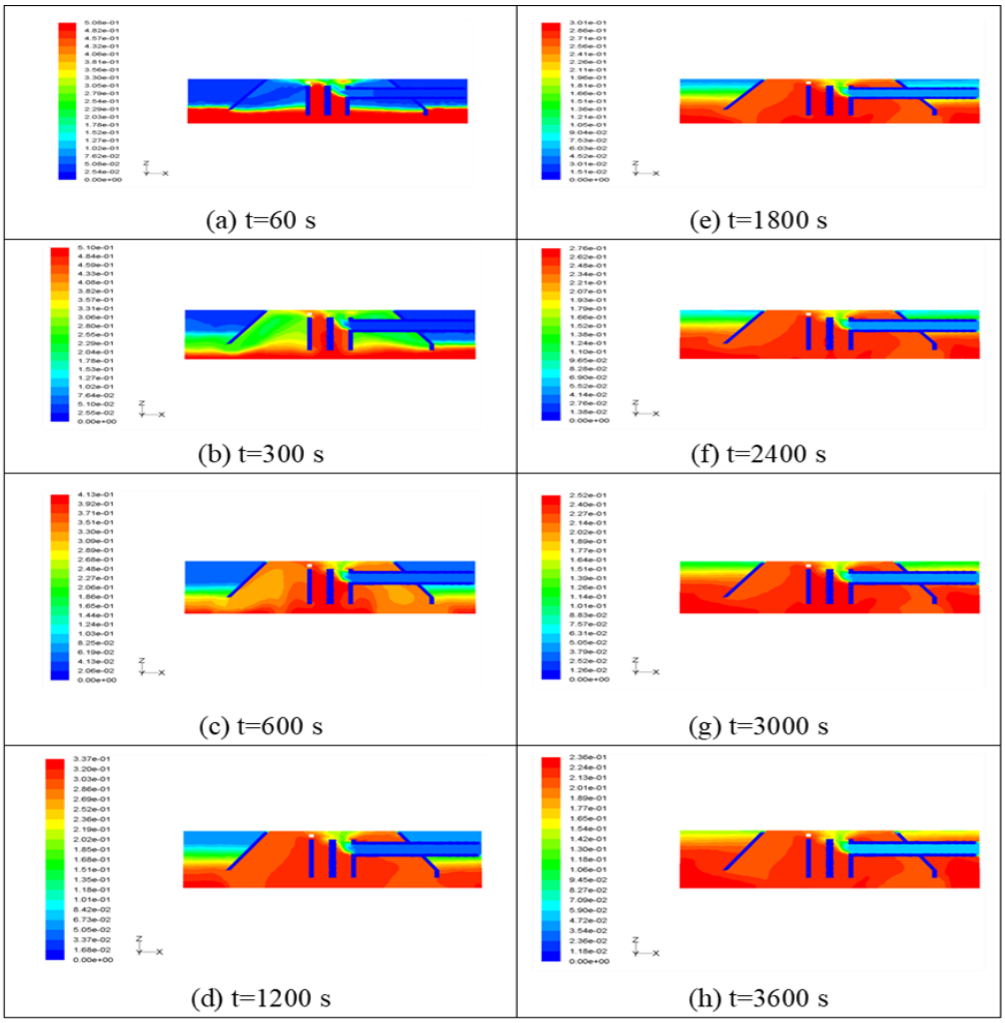

Figure 14. Change of solid volume fraction with time for NRW at plane y = 0

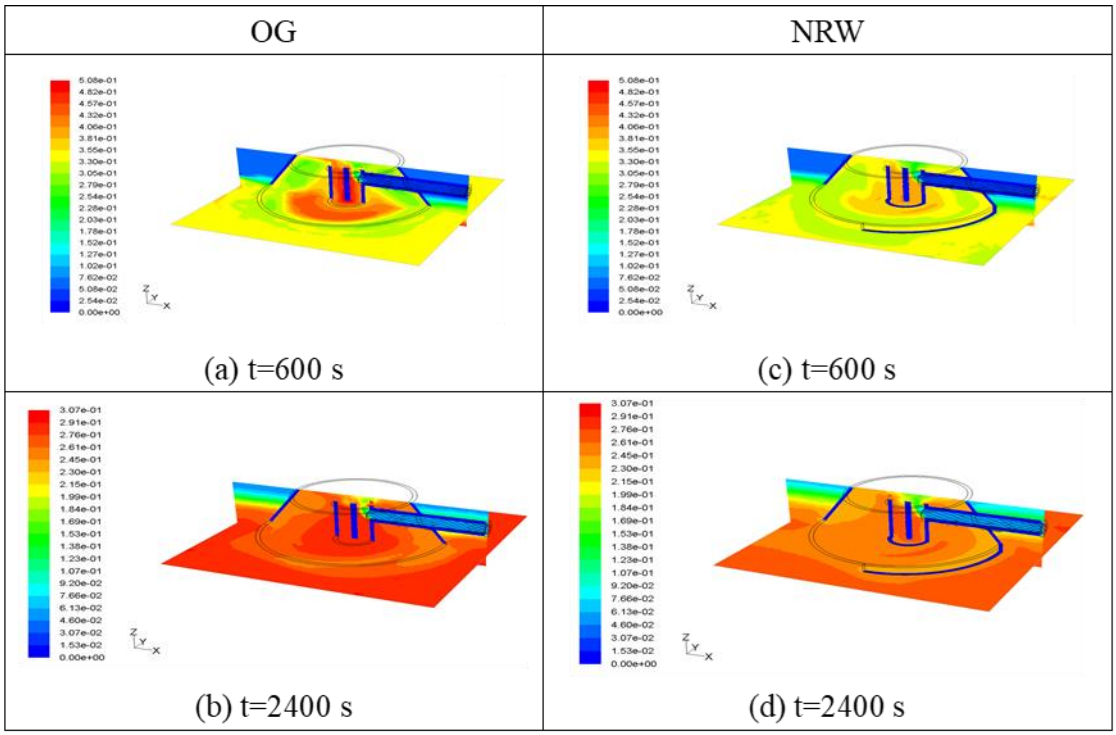

Figure 15. A comparison of solid volume fractions between OG and NRW at t = 600 and 2400 s

3.7 Viscosity formula to simulate flow field in reaction clarifier

A user-defined function (UDF) is used to define the sludge blanket viscosity formula. The Casson formula (referred to as UDFMU) is used in the study to simulate the flow field of the reaction clarifier. Figure 16 shows the solid volume fraction of OG and UDFMU as a function of time. At t = 300 s, the second reaction chamber is filled with a mixture of flocs and water, and the solid volume fraction of the reaction chamber is maintained at about 0.15 to 0.28. When t = 600 s, the high-concentration sludge blanket underneath is washed away, and the solid volume fraction of the sludge blanket is about 0.28 to 0.5. Between t = 900 s and t = 1200 s, the second reaction chamber changes from yellow to orange-red, with a medium to high concentration of about 0.27 to 0.32, and the thickness of the sludge blanket also reaches a half of the reaction hood. From Figure 16, it is found that the difference between OG and UDFMU is negligible. Therefore, the calculation of the viscosity formula is influenced by other parameters that affect the overall calculation results.

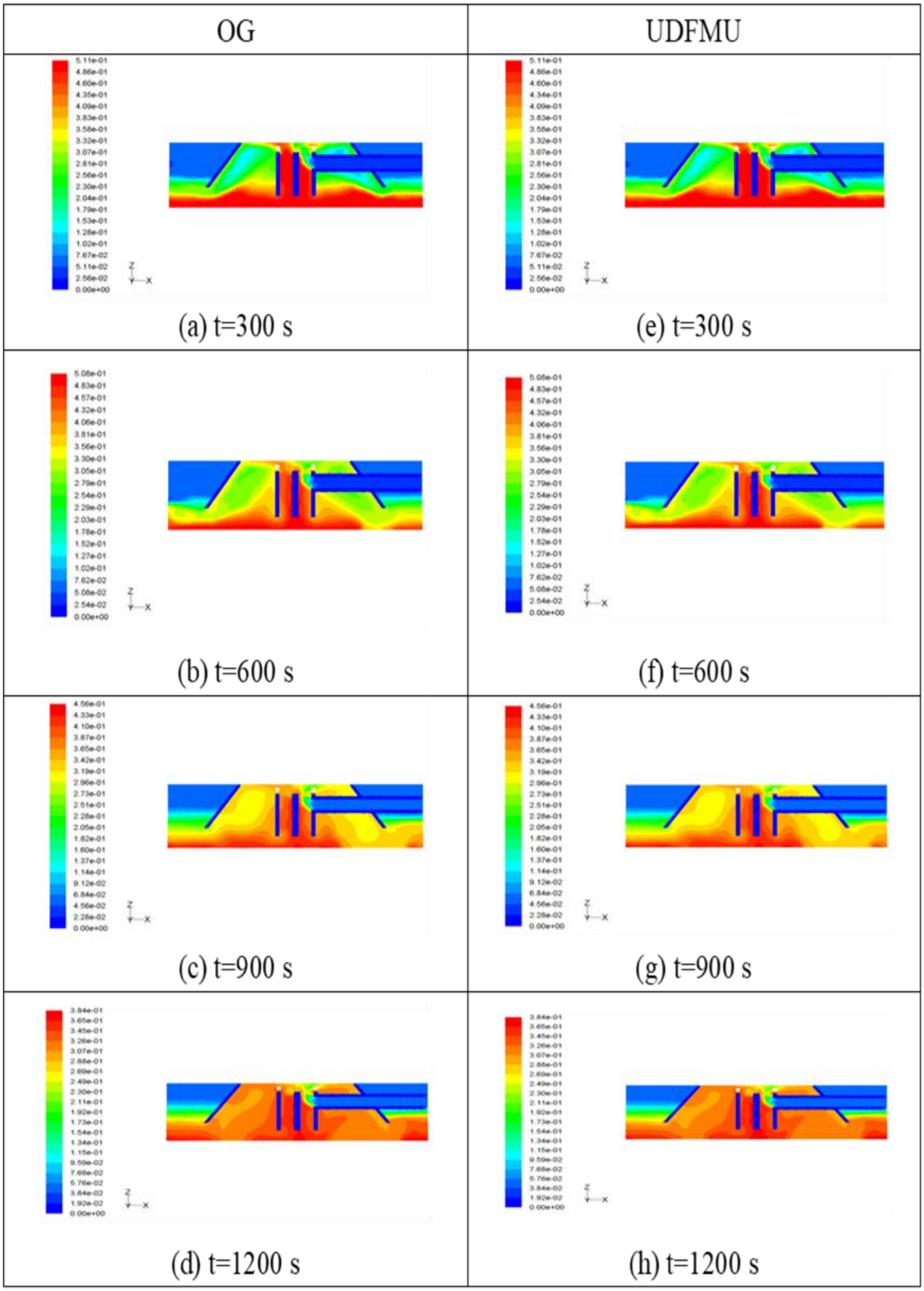

Figure 16. The change of solid volume fraction for OG and UDFMU with time

4. Conclusion

In this study, CFD model has been developed to simulate the flow field analysis and concentration changes in the reactor clarifier with the complex geometries for various situations. The collected results indicated the followings:

- In turbulent flow mode, the sludge blanket with high influent concentration rises rapidly. The effluent quality with a high influent concentration decays slowly.
- Among three speed of impeller (rad/s): 0.9 (OG), 0.3 (R03), and 0.1 rad/s (R01), the higher the speed, the larger the amount of sludge blanket at the bottom of the reaction hood that can be driven and the faster it turns.
- The higher the height of the sludge blanket, the faster the sludge blanket rises. The decline rate and quality of the effluent quality also depend on the height of the sludge blanket.
- The results of Z3 and Z3R03 shows that the sludge blanket height condition is the main key with more effect on the effluent, compared to impeller speed condition. Therefore, it is recommended that the water treatment plant should consider the initial height setting of sludge blanket.
- In the discrete phase mode, it is found that the particles of the third phase become slower when passing through the sludge blanket, which indicates that the sludge blanket may grab particles.
- The modification of the reaction hood geometry shows that uneven particle flowing on both sides of the reaction hood is improved.

References

1. Chang, C.H.; Harrison, J.F.; Huang, Y.C.(2015). Modeling Typhoon-Induced Alterations on River Sediment Transport and Turbidity Based on Dynamic Landslide Inventories: Gaoping River Basin, Taiwan. *Water* **2015**, 7, 6910–6930.
2. Zhang, Y.; Liu, P.; Xiao, L.; Chang, L.; Yan, F.; Jiang, L.(2022). Effect of Cone-Plate Clarifier Structure Parameters on Flocculation Efficiency, *Separations* 9, 6–17.
3. Kolpakova, V.; Ospanov, K.; Kuldeyev, E.; Andraka, D.(2021). Clarification of Biologically Treated Wastewater in a Clarifier with Suspended Sludge Layer. *Water* , 13, 2486–2497.
4. Su, J.; Wang, L.; Zhang, Y.; Gu, Z. A.(2019).Numerical Study on Influent Flow Rate Variations in a Secondary Settling Tank, *Processes* , 7, 884–899.
5. Head, R.; Hart, J.; Graham, N.(1997).Simulating the effect of blanket characteristics on the floc blanket clarification process. *Water Sci. Technol.* 36, 77–84.
6. Gregory, J.(1990). The role of colloid interactions in solid-liquid separation. *Water Sci. Technol.* 27, 10–17.
7. McGraw-Hill, N.Y., U.S.A, (1990).AWWA/ASCE, *Water Treatment Plant Design.* Chap. 7.
8. Diehl, S.(2008). *The solids-flux theory – Confirmation and extension by using partial differential equations. Water Res.* 42(20), 4976–4988.
9. Cui, Y.; Ravnik, J.; Steinmann, P.; Hribersek, M.(2019). Settling characteristics of nonspherical porous sludge flocs with nonhomogeneous mass distribution. *Water Res*. 158, 159–170.
10. Takacs, I.; Patry, G.G.; Nolasco, D. (1991). *A dynamic-model of the clarification thickening process. Water Res*. 25, 1263–1271.
11. Plósz, B.G.; Nopens, I.; Rieger, L.; Griborio, A.; Clercq, J.D.(2012). Vanrolleghem, P.A.; Daigger, G.T.; Takács, I.; Wicks, J.; Ekama, G.A. *A critical review of clarifier modelling: State-of-the-art and engineering practices.* WWTmod . file:///C:/Users/John%20Wu/Downloads/A_critical_review_of_clarifier_modelling_State-of-.pdf
12. De Clercq, J.; Devisscher, M.; Boonen, I.; Vanrolleghem, P.A.; Defrancq, J.(2003) *A new one-dimensional clarifier model - verification using full-scale experimental data. Water Sci. and Technol.* 47, 105–112.
13. Wett, B.(2002). *A Straight Interpretation of the Solids Flux Theory for a Three-Layer Sedimentation Model. Water Res.* 36, 2949.
14. Ekama, G.A.; Marais, P.(2004). *Assessing the Applicability of the 1D Flux Theory to Full-Scale Secondary Settling Tank Design with a 2D Hydrodynamic Model. Water Res*. 38, 495.
15. Armbruster, M.; Krebs, P.; Rodi, W.(2001). *Numerical modelling of dynamic sludge blanket behaviour in secondary clarifiers. Water Sci. and Technol.*43, 173–180.

16. Chatellier, P.; Audic, J.M.(1998).*An empirical dynamic model for waste water treatment plant clarifier simulation.* Environ. Technol.19, 725–731.
17. Xu, D.; Li, J.; Liu, J.; Ma, T.(2020). Rapid aerobic sludge granulation in an integrated oxidiation ditch with two-zone clarifiers. *Water Res*.175, 115704.
18. Caraman, S.; Luca, L; Vasiliev, I; Barbu, M.(2020). Optimal-Setpoint-Based Control Strategy of a Wastewater Treatment Process. *Processes, 8*(10),1203; **https://doi.org/10.3390/pr8101203**
19. Gao, H.; Stenstrom, M.K.(2019). Development and applications in CFD modeling for secondary settling tanks over the last three decades: a review. *Water Environ. Res.* 92, 796–820.
20. Basith, M.S.A.; Sallih, N.; Soon, W.P.K; Shibano, S.T.; Singh, R.; Sulong, M.A. (2021). Effects of Selection of Inlet Perturbations, Multiphase and Turbulence Equations on Slug Flow Characteristics Using Altair® AcuSolve™. *Processes*.9(12), 2152; https://doi.org/10.3390/pr9122152
21. Burger, R.; Karlsen, K.H.; Towers, J.D.(2005). Mathematical model and numerical simulation of the dynamics of flocculated suspensions in clarifier-thickeners. *Chem. Eng. J.* **2005**, 111, 119–134.
22. Wu, R.M.; Lee, T.H.; Yang, W.J.(2008). Study of Flow in a Blanket Clarifier Using Computational Fluid Dynamics. *J. Environ. Eng*.134, 443–455.
23. Wu, R.M.; Lee, T.H.; Yang, W.J. (2007). A study of water treatment clarifier. *Tamkang J. Sci. Eng.*10, 335–340.
24. Qi, J.; Qi, Y.; Chen, Q.; Yan, F. A.(2022). Study of Drag Reduction on Cylinders with Different V-Groove Depths on the Surface. *Water* , 14, 36–56.
25. Yu, Z.; Wang, X.; Li, W.; Chen, S.(2021). Computational Fluid Dynamics Modeling of Hollow Membrane Filtration for Concentration Polarization. *Water*.13, 3605–3614.
26. Cisneros, J.F.; Cobos, F.; Pelaez-Samaniego, M.R.; Rehman, U.; Nopens, I.(2021). Alvarado, A. Hydrodynamic Evaluation of Five Influent Distribution Systems in a Cylindrical UASB Reactor Using CFD Simulations. *Water*.13, 3141–3158.
27. Kou, J; Jiang, Z.; Cong, Y.(2021). Separation Characteristics of an Axial Hydrocyclone Separator. Processes 9(12), 2288; https://doi.org/10.3390/pr9122288
28. Zhang, J.; Yang, H.; Liu, H.; Xu, L.; Lv, Y.(2021). Pressure Fluctuation Characteristics of High-Speed Centrifugal Pump with Enlarged Flow Design. *Processes* **.**9(12), 2261; https://doi.org/10.3390/pr9122261
29. Goula, A.M.; Kostoglou, M.; Karapantsios, T.D.; Zouboulis, A.I.(2007). A CFD methodology for the design of sedimentation tanks in potable water treatment Case study: The influence of a feed flow control baffle. *Chem. Eng. J.*140, 110–121.
30. Shahrokhi, M.; Rostami, F.; Said, M.A.M.(2013). Numerical modeling of baffle location effects on the flow pattern of primary sedimentation tanks. Applied Mathematical Modelling, 37, 4486–4496.

31. Tarpagkou, R.; Pantokratoras,(2013). A *CFD methodology for sedimentation tanks: The effect of secondary phase on fluid phase using DPM coupled calculations.* Applied Mathematical Modelling,37, 3478–3494.
32. Das, S.; Bai, H.; Wu, C.; Kao, J.H.; Barney, B.; Kidd, M.; Kuettel, M.(2015). Improving the performance of industrial clarifiers using three-dimensional computational fluid dynamics. Engineering applications of computational fluid mechanics, 10, 130–144.
33. Morse, D.; Siczka, J.; Nielsen, K. (2016). Extending the McCorquodale model for 3D CFD of settling tanks and clarifiers. Proceedings of the 89th Annual Water Environment Federation Technical Exhibition and Confer.ence [CD-ROM]; Chicago, Illinois, Sept. 26–30; Water Environment Federation: Alexandria, Virginia.
34. Gao, H.; Stenstrom, M.K.(2017). Computational Fluid Dynamics Applied to Secondary Clarifier Analysis. World Environmental and Water Resources Congress 301–315.